Progress In Electromagnetics Research M, Vol. 88, 169–178, 2020

Optimizing Compensation Current to Minimize Underwater Electric Field of Ship

Qinglin Xu[1], Xiangjun Wang[1, *], Chong Xu[2], and Haiguang Wang[1]

Abstract—In order to reduce the underwater electric field generated by corrosion of ship, a boundary element method (BEM) combined with nonlinear polarization curve was employed to investigate the influence of output current of compensate anode in an electric field protection system on underwater electric field. Moreover, the BEM model was verified by physical scale modeling (PSM). The distribution characteristic of electric field and the variation trend of electric field with compensate current obtained by simulation are consistent with the experimental results. Moreover, the errors of peak-to-peak value of electric field obtained by experiment and simulation are within 20%. Compared with 0 mA compensation current, the peak-to-peak values of X component, Y component, Z component, and modulus are reduced by 52%, 70%, 72%, and 62% respectively when compensation current is 40 mA. The phenomenon of over-compensation will occur if compensation current is greater than 40 mA.

1. INTRODUCTION

Severe corrosion occurs in ship hull owing to corrosive seawater, and then corrosion electric field is generated near the hull when corrosion current flows through conductive seawater [1, 2]. With the continuous development of underwater electric field detection technology, corrosion electric field has become the signal source of new mine warfare weapon attack on ships [3]. The effects of conductivity, flow rate, depth of seawater, and other marine environmental factors on the distribution of corrosion electric field were studied [4–6]. Furthermore, the corrosion electric field of ship was simulated by equivalent electric dipole, and the electromagnetic field generated by horizontal and vertical electric dipoles in stratified media was analyzed [7–9]. In order to improve the survivability of naval vessels, it is necessary to suppress or eliminate the corrosion electric field of ship. Based on the idea of ship degaussing, offsetting the corrosion electric field by installing an electric field protection system on ship hull and the direction of compensation current is opposite to corrosion current in seawater [10].

Boundary element method and physical scale modeling are the main methods to investigate the design of ship cathodic protection and the distribution of underwater electric field [11]. The former is a method based on the weighted residual method, which converts the boundary value problem into a boundary integral equation problem and then uses the finite element discrete technique to construct linear equations [12]. BEM was first applied to anticorrosion research of offshore engineering structures in early 1980s [13]. Nowadays, it has been widely used in the simulation of cathodic protection system optimization of various marine structural parts such as oil rigs, submarine pipelines, and ships [14–17]. PSM [18] is based on scaling physical quantities such as ship's dimension and ocean environment parameters according to a certain proportion, and surface potential and underwater electric field distribution of ship are analyzed by experimental means, which has the advantages of replicating the complex geometry of ship, the same electrochemical corrosion characteristics of material as that of ship,

Received 4 November 2019, Accepted 30 December 2019, Scheduled 16 January 2020
* Corresponding author: Xiangjun Wang (nuexjwang@hotmail.com).
[1] College of Electrical Engineering, Naval University of Engineering, Wuhan 430033, China. [2] College of Education, Central China Normal University, Wuhan 430079, China.

saving time, and reducing cost, and has been applied in the design of naval ship cathodic protection in the United States, Britain, and other countries [11, 18].

Compensation current has a significant effect on underwater electric field; therefore, how to choose the appropriate compensation current is a problem that needs to be solved before the electric field protection system is installed. In this paper, the 3-DBEM was employed to establish a corrosion electrostatic field model of ship, and the nonlinear polarization curve measured by the experiment was taken as boundary condition of the model. The effect of compensation current on underwater electric field of ship was studied. Furthermore, the BEM model was verified by the PSM. The influence law of compensation current on underwater electric field and the optimal compensation current were obtained. The simulation results are in good agreement with the experimental measurement, indicating that the corrosion electric field boundary element model can effectively predict the distribution characteristic of underwater electric field of ship.

2. BOUNDARY ELEMENT METHOD

2.1. Fundamental Theory

The governing equation and boundary conditions for three-dimensional corrosion electric field are shown in Fig. 1. The homogeneous seawater medium is represented by Ω, and its boundary is composed of S_1, S_2, S_{3a}, and S_{3c} in the picture. The potential distribution of seawater domain and electrode surface is in accordance with the following Laplace equation and boundary conditions [19]:

$$\nabla^2\phi = \frac{\partial^2\phi}{\partial^2 x} + \frac{\partial^2\phi}{\partial^2 y} + \frac{\partial^2\phi}{\partial^2 z} = 0 \tag{1}$$

$$\begin{cases} \phi = \phi_0 & \text{(Constant potential boundary)} \\ I = I_0 & \text{(Constant current boundary)} \\ I_a = f_a(\phi_a) & \text{(Anodic polarization boundary)} \\ I_c = f_c(\phi_c) & \text{(Cathodic polarization boundary)} \end{cases} \tag{2}$$

where ϕ and I are the potential and current density of seawater medium and electrode surface; ϕ_0 and I_0 are the constant values of ϕ and I at the boundaries of S_1 and S_2, respectively; I_a and I_c represent the anodic current density and cathodic current density, respectively; $f_a(\phi_a)$ and $f_c(\phi_c)$ represent the anodic polarization equation and cathodic polarization equation, respectively.

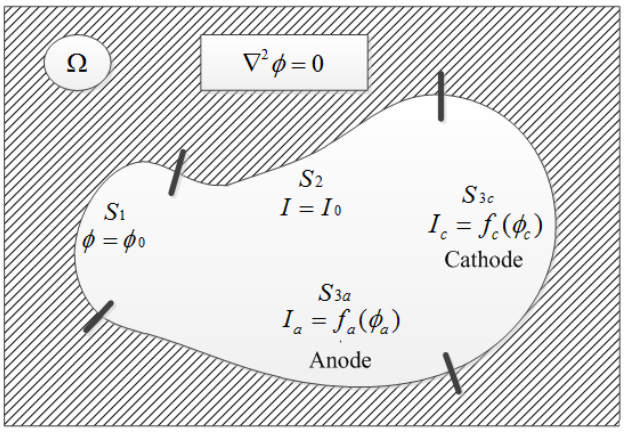

Figure 1. Governing equation and boundary condition for applying BEM to corrosion electric field.

2.2. Numerical Simulation Model

The scaled geometric model of ship in a Cartesian coordinate system was established by using Solidworks. We assume that the coating breakdown factor of hull is 2%, and hull presents a uniform

corrosion. Moreover, the impressed current cathodic protection system is closed, and two electric field compensation anodes are distributed near the propeller. The boundary element model of corrosion electrostatic field for ship was established by current distribution (boundary element) interface in the COMSOL Multiphysics. Propeller was treated as bare metal immersed in the NaCl solution, while hull was coated by the organic coating with coating breakdown factor of 2%. The solution domain and boundary conditions of the model were set as follows: (1) the infinite space was NaCl solution, and the conductivity was 4 S/m (corresponding to 3.5% NaCl solution); (2) the nonlinear polarization curve of B10 was set as the boundary condition of propeller; (3) the nonlinear polarization curve of 921A multiplied by coating breakdown factor was set as the boundary condition of hull; (4) the compensation anode is constant current boundary. The distributions of corrosion electrostatic field for different compensation currents are solved by using parametric scanning in COMSOL, and current was scanned from 0 mA to 60 mA with an interval of 10 mA. The BiCGStab iterative solver is used to solve the model. In order to be consistent with the experimental observation path, the path with point $(-8, 0.3, -0.3)$ m and $(8,\ 0.3,\ -0.3)$ m as endpoint in the vicinity of ship is selected as the observation object.

2.3. Potentiodynamic Polarization Curves

High strength low alloy 921A steel was used for the hull and rudder, and chemical composition (mass fraction, %) is as follows: C = 0.07 ~ 0.14; Si = 0.17 ~ 0.37; Mn = 0.30 ~ 0.60; S ≤ 0.015; P ≤ 0.020; Ni = 2.60 ~ 3.00; Cr = 0.90 ~ 1.20; Mo = 0.20 ~ 0.27; V = 0.04 ~ 0.10 and a Fe balance. The chemical composition of B10 copper alloy with good corrosion resistance used for the propeller is as follows (mass fraction, %): Ni = 10.02; Fe = 1.54; Mn = 0.10; P < 0.02; S < 0.02; Zn = 0.13; Pb < 0.2 and a Cu balance.

The potentiodynamic polarization curves of 921A and B10 were measured on electrochemical workstation using a three-electrode system, and the medium was NaCl solution with conductivity of 4 S/m. The working electrode was encapsulated by epoxy resin, and the sample is a cylinder with a diameter of 1.1 cm and a height of 1 cm, so the exposed area of metal is 1.0 cm^2. Before the tests, the specimens were abraded with wet SiC paper (initially 220, 600 and 1000 grades), rinsed with acetone and ethanol, and finally dried with pure nitrogen gas [6]. The reference electrode was an Ag/AgCl electrode, and the counter electrode was a platinum plate electrode with an area of 2 cm^2. The working electrode was immersed in the solution for a period of time until the open circuit potential was stabilized and then started to test. Potential was scanned from −1.1 V to 0 V, and the scanning rate is 1.0 mV/s.

The polarization curves are shown in Fig. 2, and it can be seen from the figure that the open circuit potentials of 921A and B10 are −0.68 V and −0.28 V, respectively. In practice, the hull and rudder are

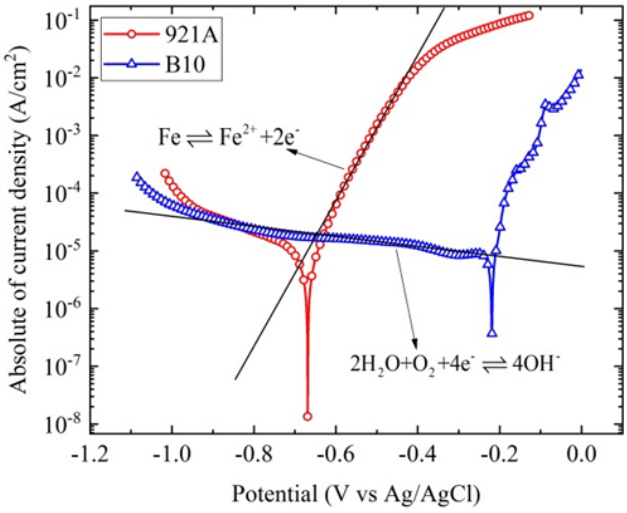

Figure 2. Polarization curves of 921A and B10.

covered with coating; therefore, the curve obtained by multiplying current density in polarization curve of 921A by coating breakdown factor (2%) is set as the boundary condition of hull immersion zone, while the propeller is exposed to seawater, so the polarization curve of B10 is set as the boundary condition of propeller directly, and the compensation anode is set as constant current boundary.

3. PHYSICAL SCALE MODELING

3.1. Experimental Condition

The experimental pool has a size of $20 \times 8 \times 2$ m and a water depth of 1 m. The inner walls of pool are made of resin-based composite material to reduce the influence of steel corrosion in concrete structure on experimental result, as shown in Fig. 3(a). Two electric field compensation anodes are arranged in the vicinity of propeller before and after, as shown in Fig. 3(b), and the output current of compensation anode is controlled by electrochemical workstation. Silver-silver chloride electrodes are used for electric field sensors, which are fixed on the glass fiber reinforced epoxy resin composite structural frame, as shown in Fig. 3(c), and ten sensors correspond to ten channel interfaces connected to the underwater electric field acquisition system. Fig. 3(d) is a schematic diagram of sensor arrangement, and $0 \sim 9$ are $0 \sim 9$# sensors in the figure. $0 \sim 8$# sensors are divided into three columns, and 9# sensor is used to measure the X component of electric field. The distance between each sensor and the adjacent sensor is 0.2 m, and the distance between the first column and the water surface is 0.3 m. The conductivity of

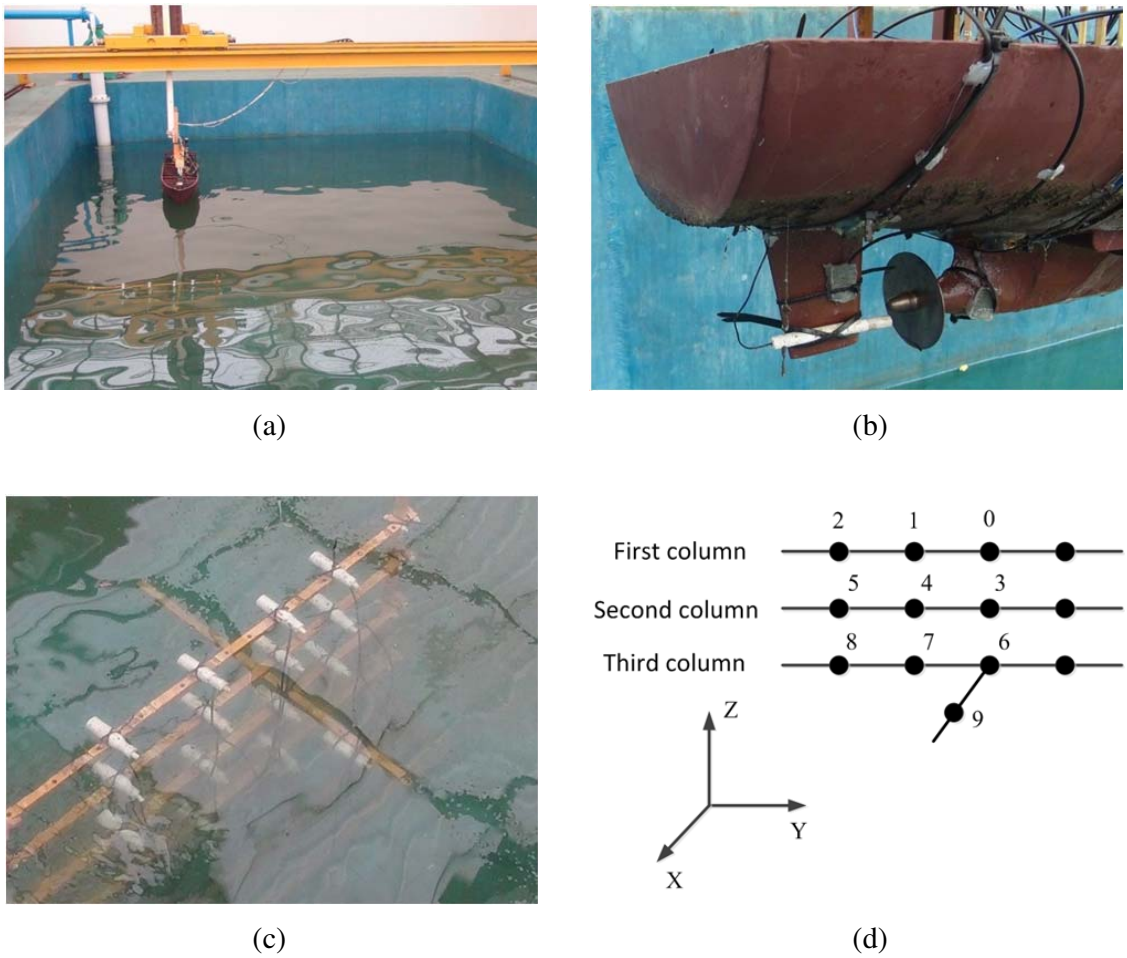

Figure 3. Physical scale modeling for (a) experimental pool, (b) position of compensation anode, (c) electric field sensor and (d) schematic diagram of sensor arrangement.

sodium chloride solution simulated seawater was adjusted to 4 S/m. The ship model was immersed in the tank for a period of time until the corrosion electric field was stabilized before starting to test, and it is driven by bridge crane through the sensor to obtain passage curve of electric field, which is used to characterize the corrosion electric field distribution around the ship model.

3.2. Calculation Method of Underwater Electric Field

The electric field acquisition system amplifies the actual result by 2000 times when collecting data and filters with a 0.5 Hz low-pass filter. The sensor measures the potential value at its location, and underwater electric field is calculated by the following formula:

$$E = \frac{U}{d} \tag{3}$$

The potential difference between two measurement points is divided by the distance between two points to approximate electric field value of the midpoint. Therefore, 6# and 9# sensors make up an electrode pair for measuring X component; 3# and 5# sensors make up an electrode pair for measuring Y component; and 1# and 7# sensors make up an electrode pair for measuring Z component. $U0 \sim U9$ represent potential values measured by $0 \sim 9\#$ sensors, respectively, and the calculation formula of three components of electrostatic field is as follows:

$$\begin{cases} EX = \dfrac{U6 - U9}{2000 \times 0.2} = \dfrac{U6 - U9}{400} \\ EY = \dfrac{U3 - U5}{2000 \times 0.4} = \dfrac{U3 - U5}{800} \\ EZ = \dfrac{U1 - U7}{2000 \times 0.4} = \dfrac{U1 - U7}{800} \end{cases} \tag{4}$$

4. RESULTS AND DISCUSSION

4.1. Simulation Results of BEM

In order to analyze the effect of compensation current on underwater electric field, a 0.5 m plane below the water surface (the horizontal plane of the second row of sensors) was selected to observe the underwater electric field distributions of ship with different compensation currents. Fig. 4 and Fig. 5 show the distributions of three components and modulus of electric field on the specified plane when compensation currents are 30 mA and 50 mA, respectively. Streamlines and arrows represent the electric field line and current direction, respectively. It can be seen from the figure that the corrosion current generated by ship in the pool flows from the bow to the stern, which is consistent with the electric dipole model of ship: the hull with anodic corrosion reaction is regarded as the positive charge of electric dipole, while the propeller with cathodic reduction reaction is regarded as the negative charge of electric dipole. Underwater electric field on the observation plane changes not only in value, but also in distribution characteristic when compensation current increases from 30 mA to 50 mA. The negative charge center of ship remains unchanged at the propeller, while the positive charge center obviously approaches the propeller, and the equivalent electric dipole moment of ship decreases accordingly, so as to reduce the underwater electric field.

The distributions of three components and modulus of electric field are analyzed more intuitively by choosing the observation path. Considering comparison with experimental results, the intersection line of 0.5 m below water surface and 0.3 m from starboard to keel is chosen as the observation path of Y and Z components, while the intersection line of 0.7 m below water surface and 0.1 m from starboard to keel is chosen as the observation path of X component and modulus. Fig. 6 shows that the distribution of electric field varies with compensation current on the specified path. When compensation current is less than 40 mA, the peak value of electric field decreases with the increase of compensation current. When compensation current is greater than 40 mA, the peak value of electric field at stern still decreases, and its position remains unchanged, while the peak value of electric field at bow moves towards stern. With the increase of compensation current, the double peaks of modulus become single peak, and the peak at

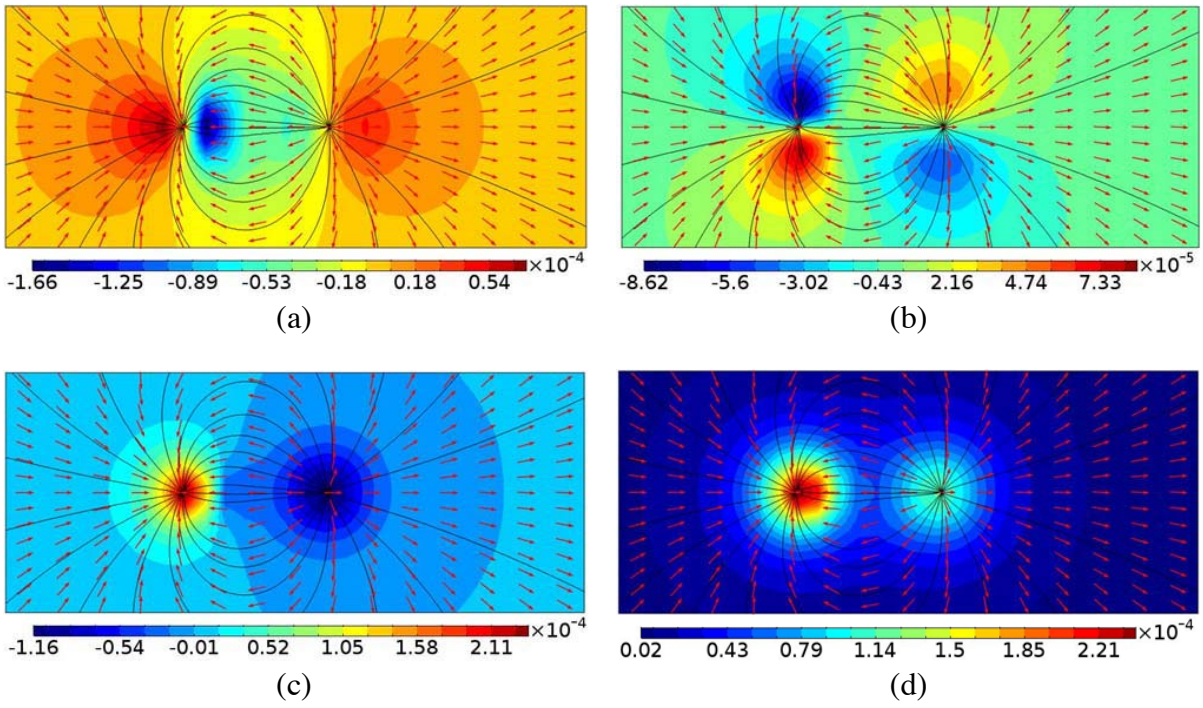

Figure 4. Electric field distribution of (a) x component, (b) y component, (c) z component and (d) modulus on the observation plane when compensation current is 30 mA.

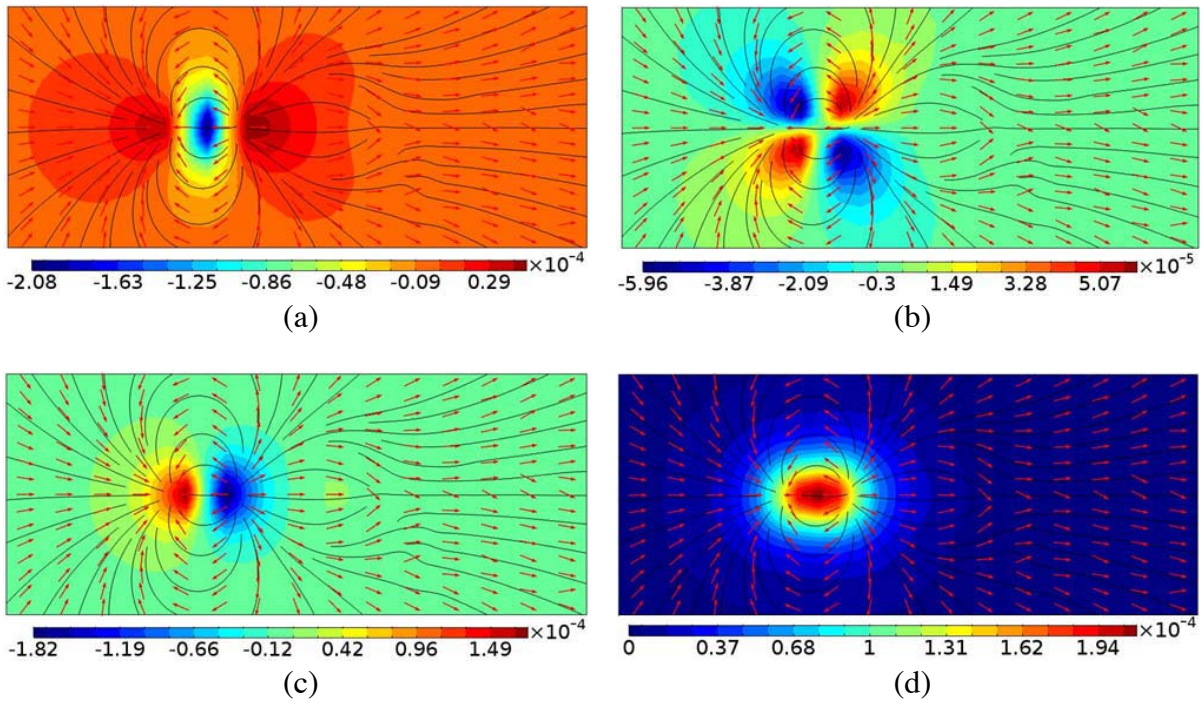

Figure 5. Electric field distribution of (a) x component, (b) y component, (c) z component and (d) modulus on the observation plane when compensation current is 50 mA.

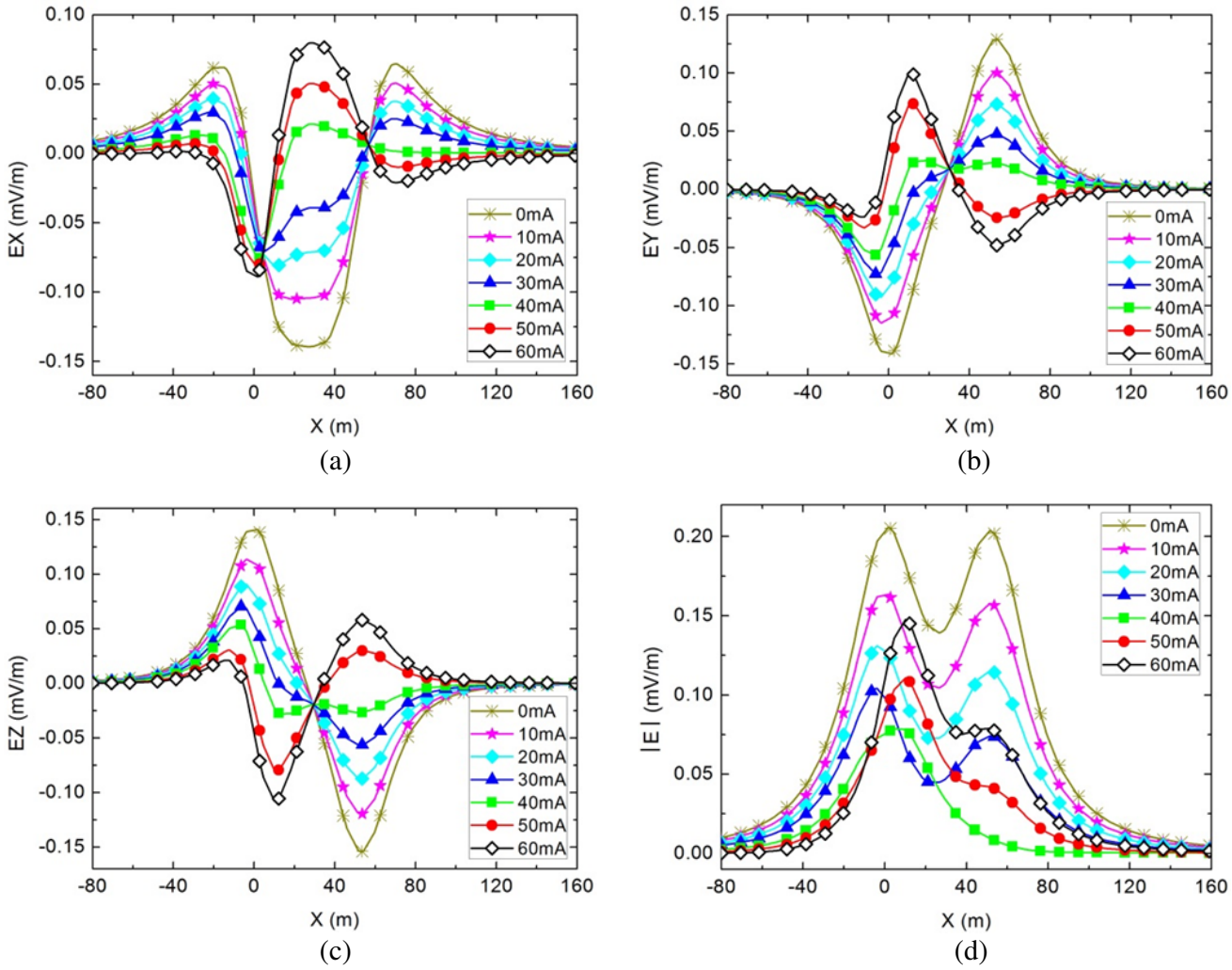

Figure 6. Electric field distribution of (a) x component, (b) y component, (c) z component and (d) modulus along the specified path varies with compensation current by BEM.

bow disappears gradually. Moreover, the peak near propeller is gradually replaced by the "anode peak" caused by compensation current, and the "anode peak" is located at position of compensation anode.

4.2. Experimental Results of PSM

Figure 7 shows experimental measurement results of electric field distribution with different compensation currents along the specified path. Table 1 shows the comparison between simulated and experimental electric field peak-to-peak values with different compensation currents. It can be seen from Fig. 7 that the distribution characteristics of three components of electric field and the variation trend of electric field with compensation current are consistent with the simulation results. The errors of peak-to-peak values of electric fields obtained by experiment and simulation are within 20%, indicating that the corrosion electric field boundary element model established in this paper can effectively predict the distribution characteristic of underwater electric field of ship. The peak-to-peak value of electric field decreases first and then increases with the increase of compensation current, and it is the smallest when compensation current is 40 mA. Furthermore, the peak-to-peak values of X component, Y component, Z component, and modulus decreased by 52%, 70%, 72%, and 62% respectively compared with no compensation current. The phenomenon of over-compensation will occur if compensation current is greater than 40 mA.

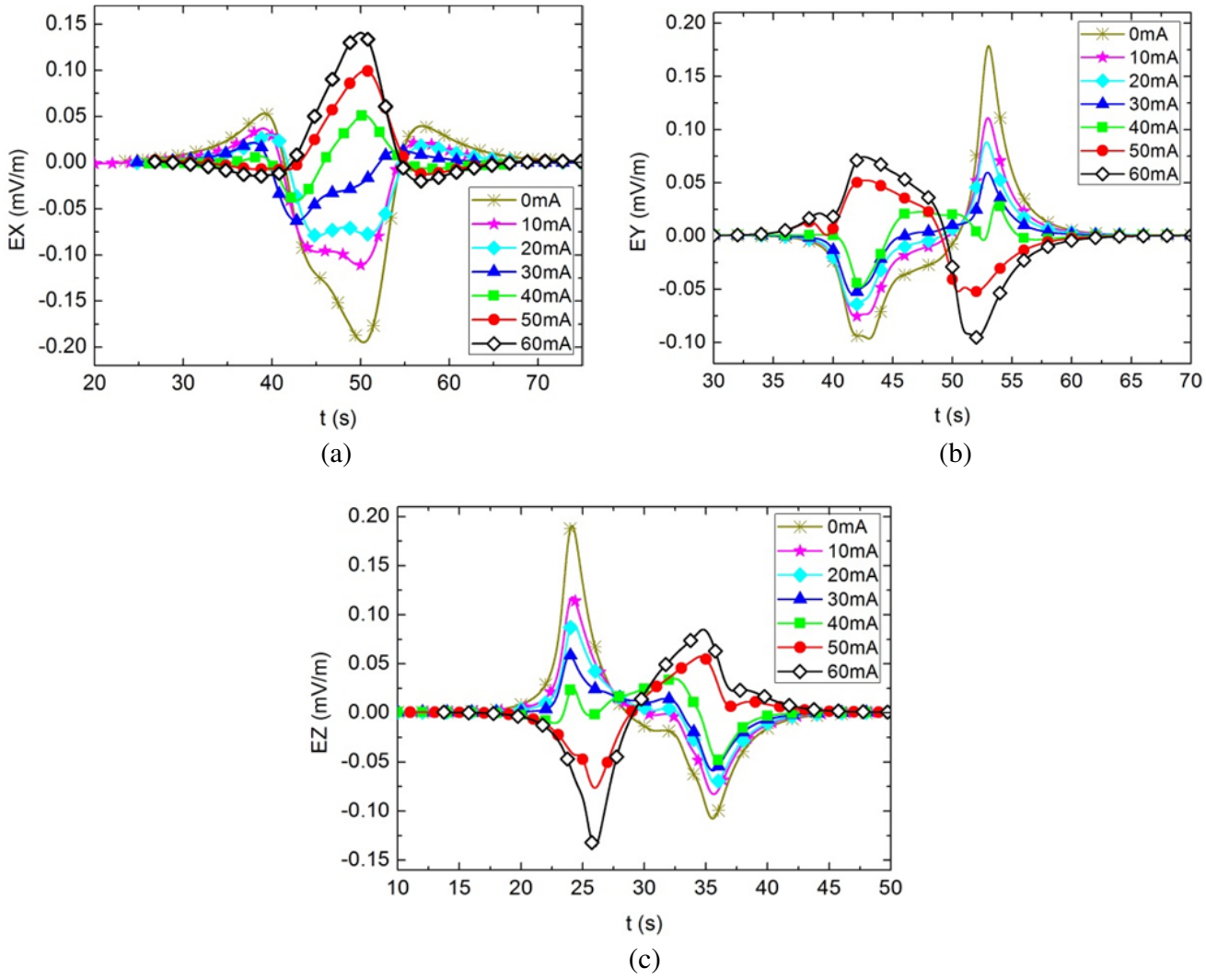

Figure 7. Electric field distribution of (a) x component, (b) y component and (c) z component along the specified path varies with compensation current by PSM.

Table 1. The comparison between simulated and experimental peak-to-peak value of electric field with different compensation current.

Current	EX (mV/m)		Error	EY (mV/m)		Error	EZ (mV/m)		Error	$\|E\|$ (mV/m)
(mA)	Simulation	Experiment	(%)	Simulation	Experiment	(%)	Simulation	Experiment	(%)	Simulation
0	0.204	0.248	−17.74	0.270	0.275	−1.82	0.295	0.312	−5.45	0.206
10	0.155	0.148	4.73	0.215	0.186	15.59	0.233	0.201	15.92	0.163
20	0.121	0.110	10.00	0.166	0.154	7.79	0.178	0.162	9.88	0.131
30	0.101	0.084	20.24	0.120	0.114	5.26	0.127	0.117	8.55	0.104
40	0.098	0.092	6.52	0.081	0.078	3.85	0.082	0.080	2.50	0.079
50	0.133	0.112	18.75	0.107	0.105	1.90	0.111	0.133	−16.54	0.111
60	0.169	0.160	5.62	0.148	0.170	−12.94	0.166	0.220	−24.54	0.148

5. CONCLUSIONS

In this paper, the influence of compensation current on underwater electric field of ship is predicted by 3-DBEM. The simulated results of BEM are compared with the experimental results of PSM. The following conclusions are drawn: the simulation results have a good agreement with the experimental ones, and the error of peak-to-peak value is within 20%, indicating that the BEM can effectively predict the distribution characteristic of underwater electric field of ship; the optimal compensation current is 40 mA, and the peak-to-peak values of X component, Y component, Z component, and modulus decrease by 52%, 70%, 72%, and 62% respectively compared with that before electric field protection; the principle of electric field protection is that compensation current makes the positive charge of equivalent electric dipole approach the negative charge, thereby reducing the equivalent electric dipole moment of ship to decrease underwater electric field.

ACKNOWLEDGMENT

This work is supported by the National Natural Science Foundation of China (Grant No. 41476153), and the authors wish to appreciate the technical support of COMSOL software company.

REFERENCES

1. Kim, Y. S., S. Seok, J. S. Lee, et al., "Optimizing anode location in impressed current cathodic protection system to minimize underwater electric field using multiple linear regression analysis and artificial neural network methods," *Engineering Analysis with Boundary Elements*, Vol. 96, 84–93, 2018.
2. Chung, H. J., C. S. Yang, G. W. Jeung, et al., "Accurate prediction of unknown corrosion currents distributed on the hull of a naval ship utilizing material sensitivity analysis," *IEEE Transactions on Magnetics*, Vol. 47, No. 5, 1282–1285, 2011.
3. Lu, J., R. Yue, and F. Yu, "Monitoring and analysis of the marine underwater electric field of the typical shallow sea area," *Near-Surface Geophysics and Environment Protection*, Vol. 36, 35–40, 2012.
4. Schaefer, D., J. Doose, M. Pichlmaier, et al., "Conversion of UEP signatures between different environmental conditions using shaft currents," *IEEE Journal of Oceanic Engineering*, Vol. 42, 1–7, 2014.
5. Kim, Y. S., S. J. Ko, S. Lee, et al., "Computational interpretation of the relation between electric field and the applied current for cathodic protection under different conductivity environments," *Metals and Materials International*, Vol. 24, No. 2, 315–326, 2018.
6. Kim, Y. S., S. K. Lee, H. J. Chung, et al., "Influence of a simulated deep sea condition on the cathodic protection and electric field of an underwater vehicle," *Ocean Engineering*, Vol. 148, 223–233, 2018.
7. Baklezos, A. T., C. D. Nikolopoulos, and C. N. Capsalis, "An equivalent dipole method with novel measurement positioning for modeling electric emissions in space missions," *Electromagnetics*, Vol. 37, No. 7, 439–453, 2017.
8. Chen, Z. Y. and S. H. Zhou, "SLF electromagnetic fields in stratified media," *Applied Mechanics and Materials*, Vol. 263, 35–38, 2012.
9. Raicevic, N. B., S. R. Aleksic, and S. S. Ilic, "Hybrid boundary element method for multi-layer electrostatic and magnetostatic problems," *Electromagnetics*, Vol. 30, No. 6, 507–524, 2010.
10. Holmes, J. J., "Application of models in the design of underwater electromagnetic signature reduction systems," *Naval Engineers Journal*, Vol. 119, No. 4, 19–29, 2007.
11. Wang, Y. and K. J. Karisallen, "Comparison of impressed current cathodic protection numerical modeling results with physical scale modeling data," *Corrosion*, Vol. 66, No. 10, 1–15, 2010.

12. Santos, W. J., J. F. Santiago, and J. C. F. Telles, "Optimal positioning of anodes and virtual sources in the design of cathodic protection systems using the method of fundamental solutions," *Engineering Analysis with Boundary Elements*, Vol. 46, 67–74, 2014.
13. Lan, Z., X. Wang, B. Hou, et al., "Simulation of sacrificial anode protection for steel platform using boundary element method," *Engineering Analysis with Boundary Elements*, Vol. 36, 903–906, 2012.
14. Kim, Y. S., J. Kim, D. Choi, et al., "Optimizing the sacrificial anode cathodic protection of the rail canal structure in seawater using the boundary element method," *Engineering Analysis with Boundary Elements*, Vol. 77, 36–48, 2017.
15. Abootalebi, O., A. Kermanpur, M. R. Shishesaz, et al., "Optimizing the electrode position in sacrificial anode cathodic protection systems using boundary element method," *Corrosion Science*, Vol. 52, 678–687, 2010.
16. Diaz, E. S. and R. Adey, "Optimising the location of anodes in cathodic protection systems to smooth potential distribution," *Advances in Engineering Software*, Vol. 36, 591–598, 2005.
17. Wang, X., Q. Xu, and J. Zhang, "Simulating underwater electric field signal of ship using the boundary element method," *Progress In Electromagnetics Research M*, Vol. 76, 43–54, 2018.
18. Ditchfield, R. W., J. N. Mcgrath, and D. J. Tighe-Ford, "Theoretical validation of the physical scale modelling of the electrical potential characteristics of marine impressed current cathodic protection," *Journal of Applied Electrochemistry*, Vol. 25, 54–60, 1995.
19. Xing, S. H., Y. Li, H. Q. Song, et al., "Optimization the quantity, locations and output currents of anodes to improve cathodic protection effect of semi-submersible crane vessel," *Ocean Engineering*, Vol. 113, 144–150, 2016.